Cavity ringdown spectroscopic detection of nitric oxide with a continuous-wave quantum-cascade laser

Anatoliy A. Kosterev, Alexander L. Malinovsky, Frank K. Tittel, Claire Gmachl, Federico Capasso, Deborah L. Sivco, James N. Baillargeon, Albert L. Hutchinson, and Alfred Y. Cho

A spectroscopic gas sensor for nitric oxide (NO) detection based on a cavity ringdown technique was designed and evaluated. A cw quantum-cascade distributed-feedback laser operating at 5.2 μm was used as a tunable single-frequency light source. Both laser-frequency tuning and abrupt interruptions of the laser radiation were performed through manipulation of the laser current. A single ringdown event sensitivity to absorption of 2.2×10^{-8} cm^{-1} was achieved. Measurements of parts per billion (ppb) NO concentrations in N_2 with a 0.7-ppb standard error for a data collection time of 8 s have been performed. Future improvements are discussed that would allow quantification of NO in human breath.

OCIS codes: 140.5960, 280.3420, 300.6320, 170.4580.

1. Introduction

Cavity ringdown spectroscopy (CRDS) is a high-sensitivity absorption-measurement technique.[1–3] It is based on measurement of the changes in relaxation time of a high-finesse optical cavity upon introducing an absorbing species. This technique was originally suggested for spectroscopic measurements with high-power pulsed lasers.[4] Subsequently, several modifications of CRDS have been developed (see, for example, Refs. 5–10). In CRDS, intensity measurements are replaced with time measurements, and hence this method is not sensitive to light-source intensity fluctuations, which enables this technique to reach a shot-noise-limited sensitivity.[10]

CRDS permits researchers to obtain an effective optical path length of several kilometers in a very small volume $V = \pi r^2 l$, where r is the mirror radius and l is the length of the optical cavity. The smallest mirror radius is defined by the acceptable level of the diffraction losses. These losses can be estimated as a fraction of the optical power in the TEM_{00} mode that misses the mirror aperture. The required mathematical relations can be found, for example, in Ref. 11. For a cavity with the geometric parameters used in this study (two identical concave mirrors separated by 37 cm and a radius of curvature of 6 m), the minimum mirror radius for 10^{-6} round-trip diffraction losses is $r = 0.36$ cm, hence $V \approx 15$ cm^3. So CRDS can be employed in the design of a compact device architecture suitable for the ultrasensitive detection of absorbing species. Of particular interest is the midinfrared spectral region, where most molecules have strong fundamental absorption bands. Field applications of such gas sensors also require a compact and intense tunable light source. Quantum-cascade (QC) distributed-feedback (DFB) lasers have the potential to be ideally suited spectroscopic sources for this application. They provide tens to hundreds of milliwatts of single-frequency radiation and can be engineered to emit at any wavelength from 4.5 to 19 μm.[12,13] Recently reported achievements include a pulsed laser with 1.15 W of single-mode peak power at 5.3 μm (Ref. 14) and a thermoelectrically cooled cw QC laser at 9.3 μm.[15] Therefore the development of CRDS based on QC DFB lasers is of considerable importance in gas-sensing applications.

Noninvasive medical diagnostics is one of the fields that can benefit from robust ultrasensitive trace-gas sensors. Some gases present in exhaled air in concentrations of parts per billion (ppb) by volume can

A. A. Kosterev (akoster@rice.edu), A. L. Malinovsky, and F. K. Tittel are with the Rice Quantum Institute, Rice University, Houston, Texas 77251-1892. C. Gmachl, F. Capasso, D. L. Sivco, J. N. Baillargeon, A. L. Hutchinson, and A. Y. Cho are with Bell Laboratories, Lucent Technologies, 600 Mountain Avenue, Murray Hill, New Jersey 07974.

Received 17 January 2001; revised manuscript received 2 May 2001.

0003-6935/01/305522-08$15.00/0

signal important physiological and pathological conditions (see, for example, Refs. 16–18. Nitric oxide (NO) detection is of particular interest.[19] In a previous paper NO detection with a QC DFB laser used in combination with either a multipass cell or a high-Q optical cavity in a cavity-enhanced spectroscopy (CES) mode was demonstrated.[20] It was found that CES does not achieve a sensitivity limit of several ppb as is required by some medical applications. Absorption spectroscopy with a multipass cell provides the required sensitivity level but has a limited time resolution because of the relatively large volume of a multipass gas cell (~3.5 l for the 100-m multipass cell used in the research described in Ref. 20).

In this paper we report a novel cw QC DFB laser-based gas-sensor architecture designed to perform CRDS detection of NO by using the same high-finesse optical cavity as is used in the CES sensor configuration reported in Ref. 20. Our approach requires a simpler design than the first CRDS experiment, with a QC DFB laser as described in Ref. 21. Paldus *et al.*[21] used a variable temperature cryostat for laser-frequency tuning with the inherent complexity and additional cost of an acousto-optic modulator to interrupt the QC laser beam. In our design both frequency tuning and the laser emission interruption were realized by manipulation of the QC laser current. With this sensor, we have demonstrated ultrasensitive detection of NO in N_2 and the detection of CO_2 in ambient air through its weak absorption near 5.2 μm ($\nu_1 + \nu_2/3\nu_2$ dyad). All the reference data for frequency-calibration and absorption-spectra simulations were taken from the HITRAN92 database. We used this earlier database edition instead of the more recent version of HITRAN96,[22] because the NO pressure-broadening coefficient in the 96 edition is set to zero in error.

2. Cavity Ringdown Spectroscopy Principles and Experimental Details

The technique we used is similar to the scheme first reported by Romanini *et al.*[5] and later applied in Ref. 21 to CRDS with a cw QC DFB laser, which consists of the following features:

1. The laser frequency is slowly scanned across the absorption line of interest;
2. One of the cavity mirrors is moved back and forth to ensure periodic, occasional coincidences of the laser frequency with a cavity mode;
3. Once such a resonance occurs and the cavity is filled, the laser beam entering the cavity is abruptly interrupted or set off resonance, and the decay rate of the exiting light is measured.

The ringdown time τ for a two-mirror cavity is defined by

$$\tau = \frac{l}{c}\frac{1}{\alpha l - \ln(R_1 R_2)^{1/2}}, \tag{1a}$$

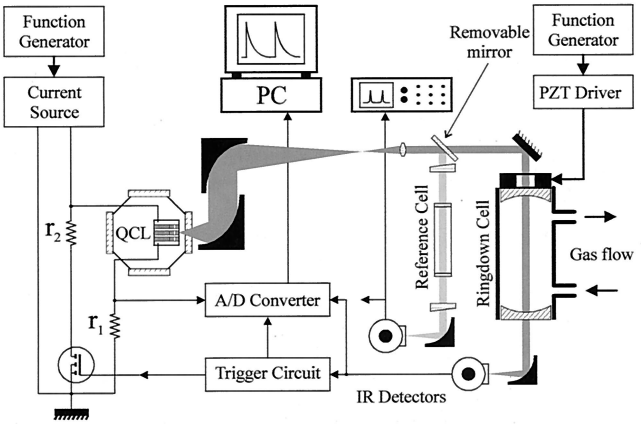

Fig. 1. Experimental setup. r_1, current monitor resistor; r_2, current-limiting resistor. Two wedged ZnSe windows shown near the reference cell were used to form an etalon for fine frequency calibration.

where l is the cavity length, c is the speed of light, R_1 and R_2 are reflectivities of the cavity mirrors, and α is the absorption coefficient of the medium inside the cavity. This expression does not take into account diffraction losses, which can be significant for high-order transverse modes or when the mirror diameter is small. In the case of $R_1 = R_2 = R \approx 1$, Eq. (1a) simplifies to

$$\tau \approx \frac{l}{c}\frac{1}{\alpha l + (1 - R)}. \tag{1b}$$

From Eq. (1a), the absorption coefficient can be determined as

$$\alpha = \frac{1}{c}\left(\frac{1}{\tau} - \frac{1}{\tau_{\text{empty}}}\right) \tag{2}$$

and its small increment as

$$\Delta\alpha = \frac{1}{c\tau}\frac{\Delta\tau}{\tau}, \tag{3}$$

where τ_{empty} is the decay constant of the cavity when evacuated.

The actual design of our CRDS setup is shown schematically in Fig. 1. We mounted the QC DFB laser on a cold finger of a liquid-nitrogen optical cryostat, and applied no active temperature control. A low-noise source supplied the laser current, and we monitored it with the 0.5-Ω resistor denoted by r_1 in Fig. 1. For absolute frequency calibration we used a reference cell filled with either CO_2 or NO. We performed fine relative calibration of the laser frequency versus the current by means of interference fringes from an airspaced etalon formed by two uncoated wedged ZnSe windows separated by 42.1 cm. The laser frequency was tunable from 1922.9 to 1920.8 cm^{-1} when the current changed from 300 mA (lasing threshold) to 660 mA. At a higher current the laser emission was multimode. With the tuning range we were able to detect NO by accessing absorption lines

at 1921.599 and 1921.601 cm^{-1} [$R(13.5)$ components of the fundamental absorption band], which could not be resolved with our experimental conditions. We also observed absorption lines of water vapor and CO_2. We collected the diverging laser radiation and collimated it with two off-axis parabolic mirrors of 76.2 mm diameter and an uncoated BaF_2 lens. We used another lens (uncoated CaF_2, $f = 50$ cm; not shown in Fig. 1) to couple the laser beam into the cavity. Two concave mirrors with a 6-m radius of curvature formed the $l = 37$-cm long, linear high-Q optical cavity. We focused radiation exiting the cell on a liquid-nitrogen-cooled photovoltaic HgCdTe detector (1-mm^2 area) with a built-in 10^4-V/A transimpedance preamplifier, dc from 20-MHz bandwidth (Kolmar Technologies Model KMPV8-1-J1/DC). The preamplifier output never exceeded 0.5 V, which is well below its saturation level of 6 V. Therefore we assumed the detector–preamplifier response to be linear. Additionally, we amplified the signal 5–20 times with an external amplifier (Stanford Research Systems SR560) and studied distortions introduced by this amplifier. We found that the measured decay time of the amplified simulated ringdown signal was only ~40 ns slower than that of the unamplified signal in the decay range of 1.3–10 μs, although the specified SR560 bandwidth is 1 MHz. This small systematic error does not noticeably influence the results.

To provide a periodic laser-cavity coupling, we applied a triangular voltage wave in parallel to three piezoelectric translators (PZT, Thorlabs PE4), making one of the cavity mirrors move back and forth. The amplitude of the mirror motion resulted in the scanning of the cavity resonances through four free spectral ranges (FSRs). When the laser frequency coincided with one of the cavity modes (TEM_{00} or a higher order), we observed a rapid increase of the detector signal (i.e., a spike). Figure 2(a) presents a typical set of spikes detected during one period of the mirror oscillations when the laser frequency was fixed and the trigger circuit was inactive. The bigger spikes correspond to the TEM_{00} cavity mode, whereas the smaller ones are due to higher-order transverse modes. Uneven spacing of TEM_{00} modes reflects PZT nonlinearity. The mirror was not attached to the PZTs but was pushed by a rubber O ring in a backward motion. This probably caused some misalignment of the cavity, which made the laser-cavity coupling less efficient on this portion of the mirror scan. The width of an individual spike [Fig. 2(b)] enables us to evaluate the laser linewidth $\Delta\nu_{QC}$, because it represents the time required for a moving cavity mode to cross the laser line. From Fig. 2, $\Delta\nu_{QC}/\mathrm{FSR} = \Delta t(\mathrm{spike})/\Delta t(\mathrm{FSR}) \approx 7.1 \times 10^{-3}$. Taking into account a $\mathrm{FSR} = c/2l = 405$ MHz, we have $\Delta\nu_{QC} \approx 3$ MHz. In this estimation we considered the spectral width of the cavity mode $\Delta\nu_{cav}$ to be negligibly small. In fact, from the measured ringdown time $\tau \approx 3.5$ μs (described below in this section) and the relation $\Delta\nu_{cav}\tau = 1/2\pi$ it follows that $\Delta\nu_{cav} \approx 45$ kHz.

When a certain level of the detector output was reached, signaling that a TEM_{00} cavity mode is coupled to the laser, a triggering circuit opened a metal-oxide semiconductor field-effect transistor (MOSFET) to shunt the laser current, thereby reducing it to a subthreshold value. At the same time, the circuit triggered an analog–digital converter (ADC, GageScope 8012), and the detector signal showing the cavity ringdown was digitized for ~30 μs and stored in computer memory. The ADC was set to a 25-MS/s sampling rate (maximum in a two-channel mode). The MOSFET was kept open for 35 μs, so that the laser radiation would not interfere with measurements of the cavity decay constant. This triggering-and-acquisition process was repeated, and consecutive ringdown transients were stacked in the ADC memory until a desired number of transients was acquired. A portion of such a data array is presented in Fig. 3(a). The results were postprocessed to fit each transient with an exponential decay function, yielding a ringdown time τ. In Fig. 3(b) a distribution is shown of the measured τ for 683 transients with an evacuated cavity and fixed laser

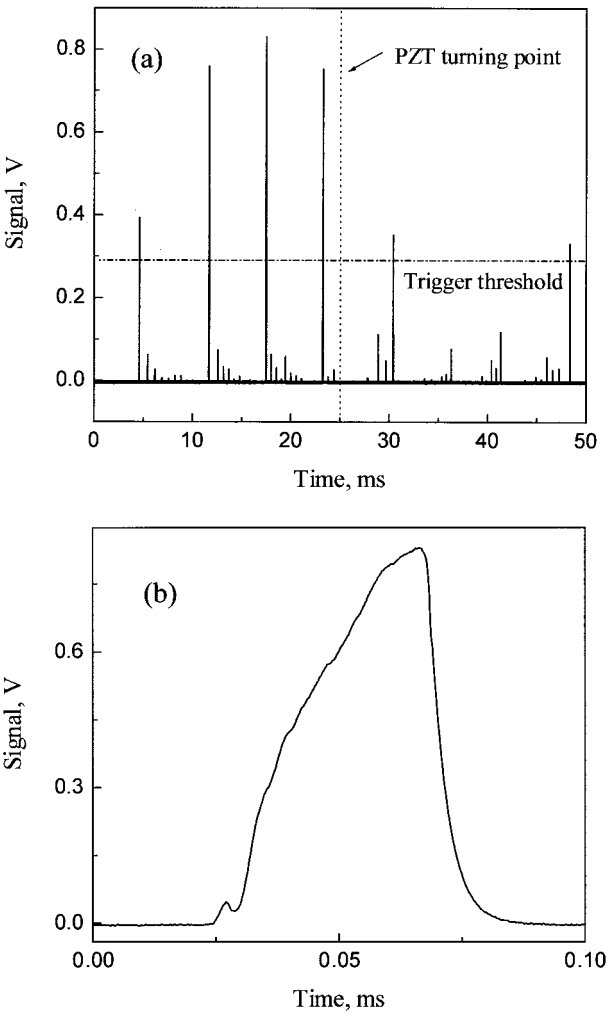

Fig. 2. (a) Laser-cavity resonances (spikes) observed during one period of the cavity mirror oscillations. The laser frequency is fixed. (b) A zoom-in of the highest spike from plot (a).

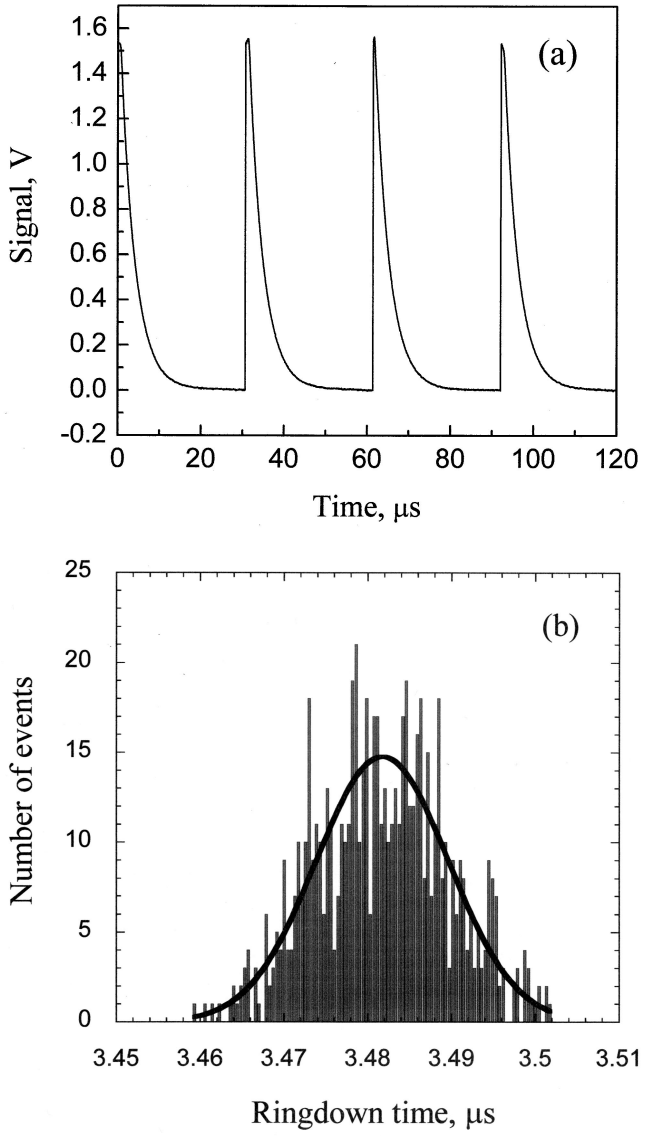

Fig. 3. (a) Sample of experimental data showing repetitive ringdown events. (b) Distribution of the ringdown times at a fixed laser frequency.

current. The distribution can be fitted with a Gaussian function, yielding $\langle\tau\rangle = 3.48$ μs and $\sigma(\tau)/\langle\tau\rangle = 2.3 \times 10^{-3}$. This means that the standard deviation of a single-shot absorption measurement is $\sigma(\alpha) = 2.2 \times 10^{-8}$ cm^{-1}, according to Eq. (3). The relative scattering of ringdown times reported in Ref. 21 was almost the same [$\sigma(\tau)/\langle\tau\rangle = 2 \times 10^{-3}$] but resulted in a lower single-shot absorption sensitivity of $\sigma(\alpha) = 7.3 \times 10^{-8}$ cm^{-1}, owing to the shorter ringdown time $\langle\tau\rangle = 0.929$ μs. An averaging of many ringdown events results in higher sensitivity (see Appendix A). Both $\sigma(\tau)$ and $\langle\tau\rangle$ varied slightly from run to run, depending on the mutual alignment of the cavity mirrors and the laser beam. The longest measured ringdown time was $\langle\tau\rangle = 3.56$ μs, from which we can conclude by use of Eq. (1a) that the actual reflectivity of the mirrors was $R = 99.965\%$. It should be noted that lower-loss mirrors have been realized, especially at visible and near-infrared wavelengths.

From a knowledge of τ and $\Delta\nu_{QC}$, we can estimate the maximum PZT frequency that can be applied without causing the amplitude of the spikes to decrease. If the cavity stays in resonance with the laser for 2τ, the exiting radiation intensity reaches $1 - 1/e^2$ of its steady-state saturation. To satisfy this condition, a sweep of the cavity resonance must occur at a speed of $d\nu/dt = \Delta\nu_{QC}/2\tau = 843$ GHz/s. We obtain a maximum PZT frequency $f_{max} = 260$ Hz, since eight FSRs are scanned for each period of the mirror oscillations. This conclusion was confirmed by our experimental observations: We did not observe any decrease of spike intensity at $f = 200$ Hz, but we observed a decrease at 300 Hz. In the spectroscopic experiments described below the PZT frequency was set to 200 Hz, which enabled maximum ringdown transient acquisitions at a 1600-Hz rate.

To acquire absorption spectra, we applied an oscillating current (triangular waveform with a dc offset) to the QC laser in order to scan a particular absorption line. The period of oscillations was typically set to 2 Hz. We extracted an ac voltage component from the current monitor resistor r_1 by subtracting a dc offset. This component was amplified and then measured by use of the second ADC channel. We measured the laser current just prior to its shutdown condition. The laser frequency at a given laser temperature is completely defined by its current, and therefore the second ADC channel provides the position of the measured ringdown time on a frequency scale. The frequency scan was found to be linear with a coefficient of 6.0 cm^{-1}/A. In previous research the laser frequency was reported to vary slightly nonlinearly with current[23–25] and linearly with temperature.[25] The linear tuning observed in this research is due to (1) a tuning range of <0.15 cm^{-1}, which could obscure a slight nonlinearity, and (2) slow tuning and a steady-state temperature for the laser chip, which is proportional to the thermal dissipation. Since the voltage applied to the laser exhibits much less relative change than the laser current, the dissipated power and hence the laser temperature scale linearly with laser current, resulting in linear frequency tuning.

After we turned the MOSFET on and off, a complete recovery of the laser frequency took ~2 ms (Fig. 4). The triggering circuit was blocked from repetitive switching during an interval of 800 μs. From Fig. 4 it can be found that the laser frequency at this moment differed from the steady-state value by only 0.14 FSR of the 421-mm-long etalon, or 1.7×10^{-3} cm^{-1}. We considered such an error in the frequency assignment to be acceptable; hence, for a PZT frequency of 200 Hz, at most every other resonance caused a registered ringdown event, and their frequency did not exceed 800 Hz.

3. Spectroscopic Measurements

The performance of this CRDS sensor was evaluated by use of three kinds of experiment:

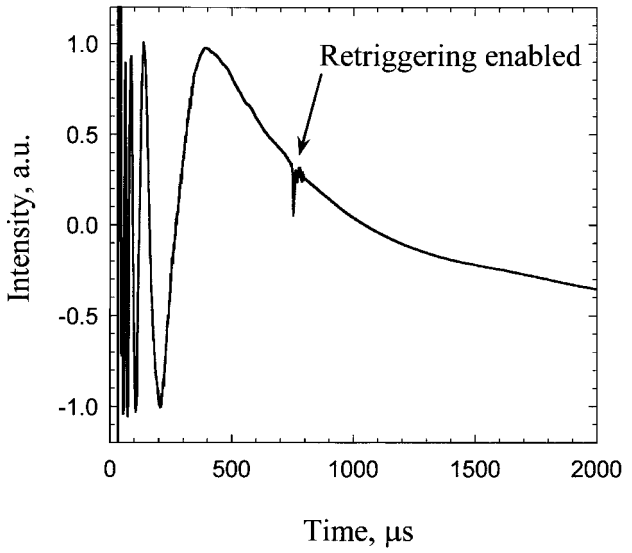

Fig. 4. Laser intensity measured after the etalon (two uncoated ZnSe surfaces 42.1 cm apart) when the laser current was reduced to a subthreshold value for 35 μs and then restored. The intensity oscillations represent etalon fringes and show a relaxation of the laser frequency when the QC laser chip heats to a steady-state value. The vertical scale was normalized to make the oscillation amplitude equal to one.

1. detection of NO at sub-ppm concentration in pure dry N_2;
2. detection of CO_2 in ambient air with use of weak absorption line at 1921.641 cm^{-1};
3. an attempt to detect NO (at the ppb level) in exhaled air samples for which a strong interference from the presence of both H_2O and especially CO_2 must also be considered.

All of the measurements were carried out at a 60-Torr total gas pressure in the cavity.

The unresolved pair of NO absorption lines at 1921.60 cm^{-1} [R(13.5) doublet] is shown in Fig. 5 as detected in a mixture with pure N_2. This mixture was originally certified by a gas manufacturer (in our case, Scott Specialty Gases) to contain 992 ppm of NO. However, the experiments were performed several months after the calibration expiration date. Besides, some NO was probably absorbed by the tubing walls. Hence, the actual NO concentration in the ringdown cell was not known *a priori*. The plot depicted in Fig. 5(a) resulted from the measurement of 1000 decays. Absorption in the cavity decreases not only the ringdown time but also the peak intensity of the light that exits the cavity when a resonance occurs. Therefore resonant spikes that appear near the peak of the relatively strong absorption line have fewer chances to reach the triggering threshold, which explains the lower density of the measured ringdown events in this region. To determine the NO concentration in this sample, we fitted the experimental data with a Voigt function. We fixed the Lorentzian and Gaussian widths to its values from HITRAN92 ($w_L = 9.07 \times 10^{-3}$ cm^{-1} = 272 MHz at

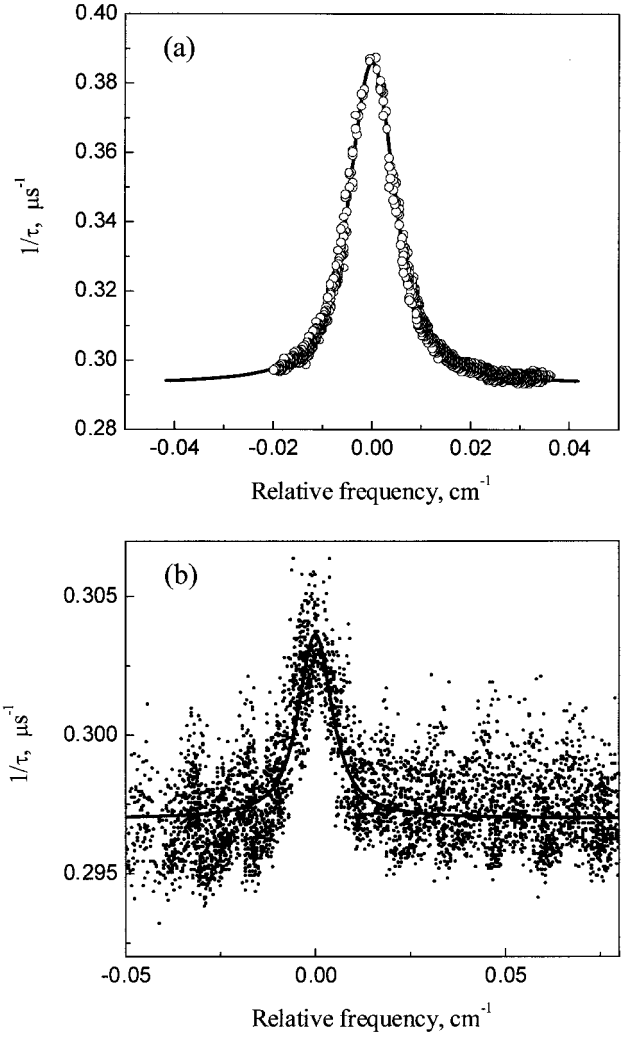

Fig. 5. Acquired absorption spectra of NO in N_2 with unresolved lines at 1921.599 and 1921.601 cm^{-1}. The solid curve shows a Voigt fit, which resulted in NO concentrations of (a) 622 ppb and (b) 48.4 ppb.

60-Torr total pressure and $w_G = 4.3 \times 10^{-3}$ cm^{-1} = 129 MHz at +25 °C). We ignored the unresolved 0.002-cm^{-1} (60 MHz) splitting of the two lines. The area of an absorption line (that is, absorbance integrated as a function of frequency) is directly proportional to concentration of the species. Comparing the area under the fitting curve [converted to cm^{-2} units by means of Eq. (2)—(cm^{-1}) of the frequency scale times (cm^{-1}) of the absorbance] to the HITRAN data for the same temperature, we found (NO) = 690 ± 2 ppb. These error limits represent only a standard deviation of the best-fit coefficient. A higher systematic error may be due to a fitting of two absorption lines with a single Voigt envelope, an inaccuracy of the reference data, and an uncertainty in the gas temperature.

Figure 5(b) shows the NO absorption detected at a lower concentration when 4000 ringdown events were acquired. The acquisition time was ~8 s. We prepared the gas sample used in this work by diluting

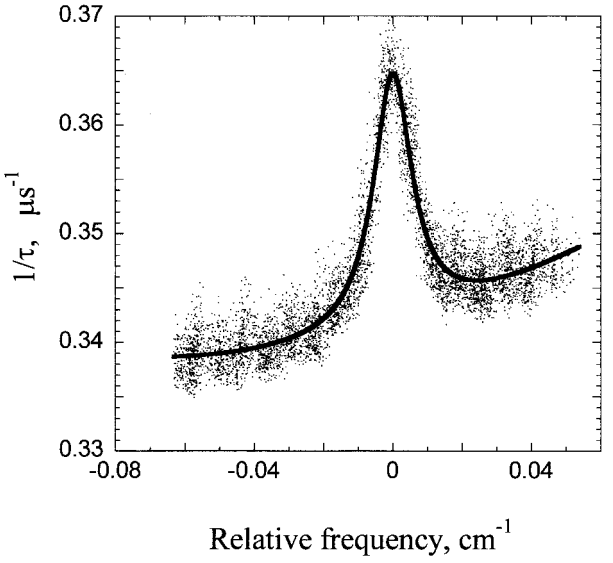

Fig. 6. CO_2 absorption line at 1921.641 cm^{-1} detected in ambient air, 60-Torr pressure. The curved baseline is caused by H_2O absorption. Solid curve shows the best fit with the Lorentzian function and a quadratic baseline. The fit resulted in a CO_2 concentration of 430 ppm.

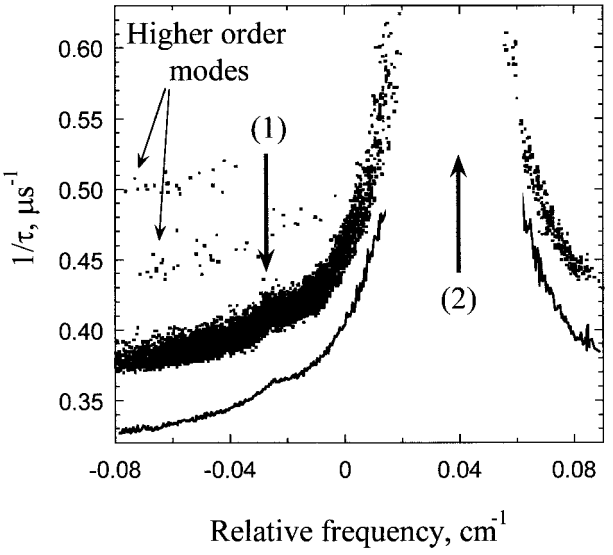

Fig. 7. Acquired spectrum of an air sample exhaled through the mouth. The breath sample was initially collected into a plastic bag and tested in the ringdown cell under a reduced pressure of 60 Torr. The 0 of the X scale corresponds to a frequency of 1921.600 cm^{-1}, where the NO absorption is expected. The two arrows indicate the CO_2 absorption lines at (1) 1921.641 cm^{-1} and (2) 1921.575 cm^{-1}. The upper array of dots shows 6000 original data points. Several points corresponding to higher-order transverse cavity modes can readily be distinguished. The lower trace represents averaged data, shifted down to 0.05 μs^{-1}.

the mixture used in previous experiments with 99.999% pure nitrogen in a continuous-flow gas-mixing system and set the dilution ratio to 18. There was no deterioration of the density of points on the top of the line, but some baseline modulation was noticeable. We believe that this modulation is caused by imperfections of the PZT motion. The mirror was not only translated but was also tilted somewhat in its back-and-forth dither motion, leading to slight changes in the cavity ringdown time. This undesirable ringdown modulation was alignment sensitive and therefore not quite reproducible from one run of measurements to another. For the data set depicted in Fig. 5(b) we evaluated $\sigma(\tau)/\langle\tau\rangle = 4.7 \times 10^{-3}$ or $\sigma(\alpha) = 4.7 \times 10^{-8}$ cm^{-1}. We fitted these data with the same Voigt envelope, with both w_L and w_G fixed. The area under the fitting curve $A = (3.53 \pm 0.05) \times 10^{-9}$ cm^{-1} yielded (NO) = 48.4 ± 0.7 ppb. We found these error limits of ±1.4% by use of the nonlinear fitting procedure. We obtained the same standard deviation $\delta A = 5 \times 10^{-11}$ cm^{-2} when the parameters of this data set (average spacing of data points around the absorption line is $\Delta\nu = 3.3 \times 10^{-5}$ cm^{-1}, the line FWHM $w = 1.1 \times 10^{-2}$ cm^{-1}, and $\sigma(\alpha) = 4.7 \times 10^{-8}$ cm^{-1}) were substituted into Eq. (A9) from Appendix A. The excess of NO concentration compared with 690 ppb divided by a dilution ratio of 18 is probably due to errors of the mixing system at low flow rates.

The CO_2 line at 1921.641 cm^{-1} detected in ambient air is shown in Fig. 6. This line corresponds to the $P(14)$ transition of the 11102 ← 00001 band in HITRAN notation and is approximately 1300 times weaker than NO absorption at 1921.60 cm^{-1}. The baseline is not flat, because the shoulder of an adjacent water absorption line is centered at 1922.341 cm^{-1}. Such a background absorption reduces the detection sensitivity of the CRDS-type gas sensors for two reasons. First, an error in α scales as $1/\tau$ for a fixed value of $\Delta\tau/\tau$, as seen from Eq. (3). Second, the decrease of the amplitude of the spikes leads to a lower signal-to-noise ratio and, in turn, to a higher $\Delta\tau/\tau$. From the difference of the vacuum ringdown constant and the baseline in Fig. 6, we can estimate a background-air absorption of $\alpha = 1.5 \times 10^{-6}$ cm^{-1} at 1921.64 cm^{-1}. Even for perfect $R = 100\%$ mirrors such an absorption would limit the ringdown time to 22 μs [see Eq. (2)]. A fitting of this data set with a Lorentzian envelope on a quadratic baseline and a comparison of the result with HITRAN-based simulations yielded a CO_2 concentration of 430 ppm. This is somewhat higher than a typical 370-ppm concentration in nonpolluted air but not surprising in a laboratory environment.

A NO concentration measurement in the air exhaled through the mouth is difficult, because it contains a high concentration of H_2O and typically ~4% of CO_2. For a pair of NO absorption lines at 1921.60 cm^{-1} that were accessible with the available QC DFB laser, CO_2 absorption lines at 1921.641 and 1921.575 cm^{-1} [R(4) from the 12202 ← 01101 hot band, HITRAN notation] hindered NO detection in a sample of air exhaled from the mouth. The acquired data are shown in Fig. 7 by dots. The solid curve shows averaged data; the spectral range was equally divided into 500 bins, and the mean value of all the

data points in each bin was plotted. A better spectral strategy would be to detect NO through another pair of absorption lines at, e.g., 1903.123 and 1903.134 cm^{-1} [R(7.5)]. These lines are free from interfering H_2O and CO_2 absorption and are more than three times stronger. The use of this pair of lines would make it possible to measure NO concentration levels of below 5–10 ppb that are typical for mouth-exhaled air.

5. Conclusions

We have demonstrated that the CRDS technique by use of current control of a cw QC DFB laser can be applied to sensitive-absorption spectroscopy in the mid-infrared range. The demonstrated sensitivity can be considerably improved by implementation of the following measures:

1. Ensure less ripple and drift for the QC DFB laser current.
2. Improve the design of a PZT mirror mount to eliminate the decay-time dependence on the mirror position.
3. Use an improved QC laser cryostat design to avoid drift of the laser beam during liquid nitrogen boil-off.
4. Use a QC laser capable of targeting the NO line pair at 1903.123 or 1903.134 cm^{-1} [$R(7.5)$], which is desirable to detect NO in exhaled air. These lines are free of CO_2 and H_2O interference and also are more than three times stronger than the pair at 1921.60 cm^{-1} used in this research.

At this time, we obtained a sensitivity of 0.7-ppb NO in pure N_2 with 4000 ringdown events. However, with the proposed improvements implemented, we estimate that it would be possible to detect NO in exhaled air down to sub-ppb levels with the acquisition of only 1000 ringdown events. At a laser shutdown rate of ~500 Hz this requires only 2 s of time plus mathematical postprocessing, which can be fast with optimum software. With the expected development of near-room-temperature cw QC lasers and further progress in ultralow-loss mid-infrared mirror technology, CRDS offers the potential for the design of compact ultrasensitive gas sensors.

Appendix A: Sensitivity of Spectroscopic Detection

To derive the relations between a single-point absorption-measurement error and an error in the integrated absorption line intensity that is proportional to the absorbing species concentration, we make two simplifying assumptions:

- the position and shape of the absorption line of interest is known;
- the baseline is completely defined and therefore can be subtracted prior to further data analysis.

The task of determining the line intensity is then reduced to finding the best-fit coefficient A:

$$y_i = Ag(\nu_i), \tag{A1}$$

where y_i is an experimentally measured absorption at frequency ν_i. For convenience, we can consider $g(\nu)$ normalized by the condition

$$\int g(\nu)\mathrm{d}\nu = 1. \tag{A2}$$

If υ and y are expressed in cm^{-1}, then $g(\upsilon)$ has a dimension of cm and $(A) = cm^{-2}$. The coefficient A describes the absorption line area, i.e., an integral of the absorption coefficient over the whole spectral range. If we denote $g(\nu_i) = x_i$, then from linear fit theory

$$A = \frac{\sum_{i=1}^{n} x_i y_i}{\sum_{i=1}^{n} x_i^2}, \tag{A3}$$

$$(\delta A)^2 = \frac{1}{n-1}\frac{\sum_{i=1}^{n}(y_i - Ax_i)^2}{\sum_{i=1}^{n} x_i^2}. \tag{A4}$$

Here δA is a standard error in A, which defines the accuracy and sensitivity of the measurements; $n \gg 1$ is the number of data points. The points υ_i are quasi-homogeneously distributed over the scan range $\Delta\Omega$, and we denote the average spacing as $\langle \nu_i - \nu_{i-1} \rangle = \Delta\Omega/n = \Delta\upsilon$. If it is assumed that individual measurements are independently scattered around true values with a standard error of σ, we have

$$\frac{1}{n-1}\sum_{i=1}^{n}(y_i - Ax_i)^2 = \frac{n}{n-1}\sigma^2 \approx \sigma^2, \tag{A5}$$

$$\sum_{i=1}^{n} x_i^2 = \sum_{i=1}^{n} g^2(\nu_i) \approx \frac{1}{\Delta\nu}\int g^2(\nu)\mathrm{d}\nu, \tag{A6}$$

$$\delta A \approx \sigma\left[\Delta\nu \Big/ \int g^2(\nu)\mathrm{d}\nu\right]^{1/2}. \tag{A7}$$

For a Lorentzian line shape,

$$\int g^2(\nu)\mathrm{d}\nu = \left(\frac{2}{\pi}\right)^2 \int \frac{w^2}{(4\nu^2 + w^2)^2}\,\mathrm{d}\nu = \frac{1}{\pi w}, \tag{A8}$$

and Eq. (A7) becomes

$$\delta A_L = \sigma(\pi\Delta\nu w)^{1/2}, \tag{A9}$$

where w equals the FWHM of the line envelope.

The authors thank Robert F. Curl for useful discussions. Financial support of the research performed by the Rice group was provided by the

National Aeronautics and Space Administration, the Institute for Space Systems Operations, the Texas Advanced Technology Program, the National Science Foundation, and the Welch Foundation. The research performed at Bell Laboratories was partially supported by DARPA/U.S. Army Research Office under grant DAAD 19-00-C-0096.

References

1. J. J. Scherer, J. B. Paul, A. O'Keefe, and R. J. Saykally, "Cavity ringdown laser absorption spectroscopy: history, development, and application to pulsed molecular beams," Chem. Rev. **97,** 25–52 (1997).
2. K. W. Busch and M. A. Busch, eds., *Cavity Ring-Down Spectroscopy: an Ultratrace-Absorption Measurement Technique*, Vol. 720 of the American Chemical Society Symposium Series (American Chemical Society, Washington, D.C., 1999).
3. G. Berden, R. Peeters, and G. Meijer, "Cavity ring-down spectroscopy: experimental schemes and applications," Int. Rev. Phys. Chem. **19,** 565–607 (2000).
4. A. O'Keefe and D. A. G. Deacon, "Cavity ring-down optical spectrometer for absorption measurements using pulsed laser sources," Rev. Sci. Instrum. **59,** 2544–2551 (1988).
5. D. Romanini, A. A. Kachanov, N. Sadeghi, and F. Stoeckel, "CW cavity ring down spectroscopy," Chem. Phys. Lett. **264,** 316–322 (1997).
6. R. Engeln, G. Berden, R. Peeters, and G. Meijer, "Cavity enhanced absorption and cavity enhanced magnetic rotation spectroscopy," Rev. Sci. Instrum. **69,** 3763–3769 (1998).
7. M. Mürtz, B. Frech, and W. Urban, "High-resolution cavity leak-out absorption spectroscopy in the 10-μm region," Appl. Phys. B **68,** 243–249 (1999).
8. Y. He and B. Orr, "Ringdown and cavity-enhanced absorption spectroscopy using a continuous-wave tunable diode laser and a rapidly swept optical cavity," Chem. Phys. Lett. **319,** 131–137 (2000).
9. M. D. Levenson, B. A. Paldus, T. G. Spence, C. C. Harb, R. N. Zare, M. J. Lawrence, and R. L. Byer, "Frequency-switched heterodyne cavity ringdown spectroscopy," Opt. Lett. **25,** 920–922 (2000).
10. T. G. Spence, C. C. Harb, B. A. Paldus, R. N. Zare, B. Willke, and R. L. Byer, "A laser-locked cavity ring-down spectrometer employing an analog detection scheme," Rev. Sci. Instrum. **71,** 347–353 (2000).
11. A. E. Siegman, *Lasers* (University Science, Mill Valley, Calif., 1986).
12. F. Capasso, C. Gmachl, R. Paiella, A. Tredicucci, A. L. Hutchinson, D. L. Sivco, J. N. Baillargeon, A. Y. Cho, and H. C. Liu, "New frontiers in quantum cascade lasers and applications," IEEE J. Sel. Top. Quantum Electron. **6,** 931–946 (2000).
13. C. Gmachl, F. Capasso, R. Köhler, A. Tredicucci, A. L. Hutchinson, D. L. Sivco, J. N. Baillargeon, and A. Y. Cho, "The seeability of semiconductor lasers," IEEE Circuits and Devices, **16,** 10–18 (2000).
14. D. Hofstetter, M. Beck, T. Aellen, and J. Faist, "High-temperature operation of distributed feedback quantum-cascade lasers at 5.3 μm," Appl. Phys. Lett. **78,** 396–398 (2001).
15. D. Hofstetter, M. Beck, T. Aellen, J. Faist, U. Oesterle, M. Ilegems, E. Gini, and H. Melchior, "Continuous wave operation of a 9.3 μm quantum cascade laser on a Peltier cooler," Appl. Phys. Lett. **78,** 1964–1966 (2001).
16. M. Phillips, "Breath tests in medicine," Sci. Am. **267,** 74–79 (1992).
17. J. C. de Jongste and K. Alving, "Gas Analysis," Am. J. Respir. Crit. Care Med. **162,** 235–275 (2000).
18. N. Wilson and S. Pedersen, "Inflammatory markers in clinical practice," Am. J. Respir. Crit. Care Med. **162,** 485–515 (2000).
19. E. Culotta and D. E. Koshland, "No news is good news," Science **258,** 1862–1865 (1992).
20. L. Menzel, A. A. Kosterev, R. F. Curl, and F. K. Tittel, "Spectroscopic detection of biological NO with a quantum cascade laser," Appl. Phys. B **72,** 859–863 (2001).
21. B. A. Paldus, C. C. Harb, T. G. Spence, R. N. Zare, C. Gmachl, F. Capasso, D. L. Sivco, J. N. Baillargeon, A. L. Hutchinson, and A. Y. Cho, "Cavity ringdown spectroscopy using mid-infrared quantum-cascade lasers," Opt. Lett. **25,** 666–668 (2000).
22. L. S. Rothman, C. P. Rinsland, A. Goldman, S. T. Massie, D. P. Edwards, J.-M. Flaud, A. Perrin, C. Camy-Peyret, V. Dana, J.-Y. Mandin, J. Schroeder, A. McCann, R. R. Gamache, R. B. Wattson, K. Yoshino, K. V. Chance, K. W. Jucks, L. R. Brown, V. Nemtchinov, and P. Varanasi, "The HITRAN molecular spectroscopic database and HAWKS (HITRAN Atmospheric Workstation): 1996 edition," J. Quant. Spectrosc. Radiat. Transfer **60,** 665–710 (1998).
23. S. W. Sharpe, J. F. Kelly, J. S. Hartman, C. Gmachl, F. Capasso, D. L. Sivco, J. N. Baillargeon, and A. Y. Cho, "High-resolution (Doppler-limited) spectroscopy using quantum-cascade distributed-feedback lasers," Opt. Lett. **23,** 1396–1398 (1998).
24. A. A. Kosterev, R. F. Curl, F. K. Tittel, C. Gmachl, F. Capasso, D. L. Sivco, J. N. Baillargeon, A. L. Hutchinson, and A. Y. Cho, "Effective utilization of quantum-cascade distributed-feedback lasers in absorption spectroscopy," Appl. Opt. **39,** 4425–4430 (2000).
25. A. A. Kosterev, F. K. Tittel, C. Gmachl, F. Capasso, D. L. Sivco, J. N. Baillargeon, A. L. Hutchinson, and A. Y. Cho, "Trace-gas detection in ambient air with a thermoelectrically cooled, pulsed quantum-cascade distributed feedback laser," Appl. Opt. **39,** 6866–6872 (2000).